Phys. Status Solidi RRL **3**, No. 2, 40–42 (2009) / **DOI** 10.1002/pssr.200802250

pss +++rapid research letters+++
www.pss-rapid.com

Hot spots in multicrystalline silicon solar cells: avalanche breakdown due to etch pits

J. Bauer[*,1], J.-M. Wagner[1], A. Lotnyk[1], H. Blumtritt[1], B. Lim[2], J. Schmidt[2], and O. Breitenstein[1]

[1] Max-Planck-Institut für Mikrostrukturphysik, Weinberg 2, 06120 Halle, Germany
[2] Institut für Solarenergieforschung Hameln/Emmerthal (ISFH), Am Ohrberg 1, 31860 Emmerthal, Germany

Received 17 November 2008, revised 4 December 2008, accepted 5 December 2008
Published online 10 December 2008

PACS 61.72.Lk, 68.37.Hk, 68.37.Lp, 77.22.Jp, 84.60.Jt

[*] Corresponding author: e-mail jbauer@mpi-halle.mpg.de, Phone: +49-345-5582 979, Fax: +49-345-5511223

Multicrystalline silicon solar cells typically show hard breakdown beginning from about −13 V bias, which leads to the well-known hot-spot problem. Using special lock-in thermography techniques, hard breakdown has been found to occur in regions of avalanche multiplication. A systematic study of these regions by various electron microscopy techniques has shown that the avalanche breakdown occurs at cone-shaped holes, located at dislocations and caused by acidic texture etch. At their bottom, these etch pits lead to a strongly curved p–n junction exhibiting an electrostatic tip effect which quantitatively explains the field enhancement needed for enabling avalanche breakdown.

Solar cells whose breakdown current exceeds a certain limit cannot be used because such cells may thermally damage the module in case of unintentional reverse biasing by local shading (hot-spot problem [1]). In order to reduce the number of off-specification cells, the reason for the high reverse currents must be identified. The physical mechanisms leading to breakdown of reverse-biased p–n junctions are internal field emission (Zener effect) and impact ionization (avalanche effect). They exhibit a characteristic temperature dependence, which can be used for their identification: for internal field emission the current increases slightly with rising temperature due to band-gap lowering, but it decreases considerably for impact ionization due to increased phonon scattering. Moreover, multiplication of photo-generated carriers takes place only for avalanche breakdown [2]. Both mechanisms require a certain electric field strength, which normally is not reached in standard multicrystalline (mc) Si solar cells. According to that field strength, however, the breakdown voltage should be four times higher than observed in practice [3].

In this letter, we present a systematic study of the breakdown mechanism in commercial, $156 \times 156\ \mathrm{mm}^2$ p-type base mc-Si solar cells. We employ special lock-in thermography (LIT) imaging techniques to identify the type of breakdown occurring at the hot spots, and various electron microscopy techniques to reveal the microscopic nature of the breakdown sites. The cells investigated were free from ohmic shunts. A typical reverse current–voltage characteristic is shown in Fig. 1, given for two different temperatures.

At lower reverse voltages, only weak currents occur, which up to approximately −13 V increase only slightly (pre-breakdown). Beyond −13 V, however, a steep current increase is observed, which is typical for a hard breakdown. For the solar cells under investigation, the pre-breakdown current increases with temperature, whereas the hard-breakdown current decreases (for a given voltage). This indicates that in general, different breakdown mechanisms are involved, a fact which also other authors have observed, using electroluminescence (EL) at reverse bias [4].

Lock-in thermography has been established as a standard technique for locating and characterizing leakage currents in solar cells [5]. For the investigation of breakdown currents we have recently proposed several LIT-based imaging techniques [6], performed either in the dark (DLIT) or under illumination (ILIT). In all these techniques, the −90° LIT signal, which can be interpreted quantitatively [7], is used. The temperature variation of the current at a given bias voltage is displayed by the Temperature-Coef-

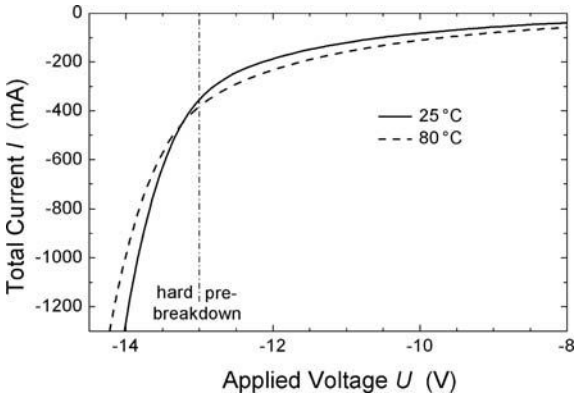

Figure 1 Total current vs. applied reverse voltage of a standard mc-Si solar cell at two different temperatures, showing pre- (zero to approx. –13 V) and hard breakdown regions (beyond –13 V).

ficient-DLIT (TC-DLIT) image, which represents a normalized central-difference derivative related to the midpoint temperature T_{mid} between the two measurement temperatures. The multiplication of photo-generated carriers (possibly occurring at avalanche breakdown sites) is displayed by the Multiplication-Factor-ILIT (MF-ILIT) image, which is obtained from two ILIT measurements with different constant reverse voltages and pulsed homogeneous illumination (for details see Refs. [6] and [8]).

The dark regions in the EL image shown in Fig. 2a correspond to regions of lower minority carrier lifetime due to the presence of recombination-active defects. However, the hard-breakdown currents observed at –14 V reverse voltage (see circles in the DLIT image Fig. 2b, obtained from a cell adjacent to that of Fig. 2a) predominantly flow in areas with long lifetimes and are therefore not correlated with these defects. These currents decrease with rising temperature, as can be seen from their negative temperature coefficient shown in Fig. 2c. Furthermore, Fig. 2d shows that multiplication of photo-generated carriers occurs in the same places where the hard-breakdown currents flow (see circles). Altogether, we conclude that impact ionization should be the conduction mechanism relevant for the hard breakdown. However, the question remains as to how the necessary field strength can be reached at the observed breakdown voltage.

Usually, avalanche breakdown occurs at specific local sites [9] where it causes so-called microplasmas [10]. Only structurally perfect p–n junctions are nearly free from microplasmas [11]. However, the spatial resolution of MF-ILIT images is not sufficient to localize single microplasma sites. EL imaging has been shown to locate breakdown sites with high spatial resolution [12]. Yet conventional reverse-bias EL investigations cannot distinguish between avalanche and Zener breakdown sites. Therefore, we have used electron-beam-induced current (EBIC) measurements at various reverse voltages for a microscopic investigation of areas showing carrier multiplication (see square in Fig. 2d). For eliminating the dc leakage current, these measurements were performed in ac-coupled lock-in

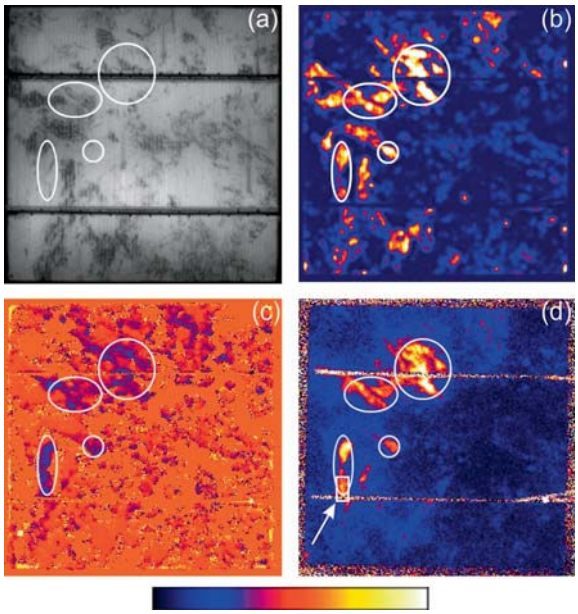

Figure 2 (online colour at: www.pss-rapid.com) EL image at forward bias (a), room-temperature DLIT image at –14 V (b), TC-DLIT image at –14 V, corresponding to T_{mid} = 32.5 °C (ΔT = 15 K) (c), and room-temperature MF-ILIT image at –15 V (d). The colour scale corresponds to the range –6 ... 60 mK for the DLIT, –6 ... + 4%/K for the TC-DLIT, and 1.0 ... 3.0 for the MF-ILIT image. In (c), regions with very weak thermal signal are set to zero [6]. The square in (d) indicated by the arrow marks the region investigated by EBIC (Fig. 3).

mode [13], thereby obtaining a significantly better image quality than in [14]. Typical results are shown in Fig. 3.

Carrier multiplication occurs where the EBIC signal at –15 V (Fig. 3b) is significantly larger than at 0 V (for which the image shows a grain boundary, cf. Fig. 3a). This

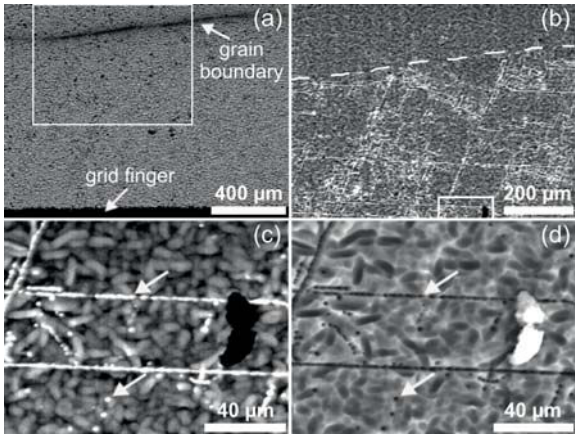

Figure 3 AC-coupled lock-in EBIC images at 0 V (a) and –15 V reverse bias (b) of the detail marked in Fig. 2d; (b) shows the region marked in (a) and the dashed line in (b) indicates the grain boundary. The part marked by the square in (b) is scanned at –15 V in higher magnification in (c). An SE image of the same part is shown in (d). Arrows in (c) and (d) indicate corresponding avalanche sites and etch pits, respectively [8, 13].

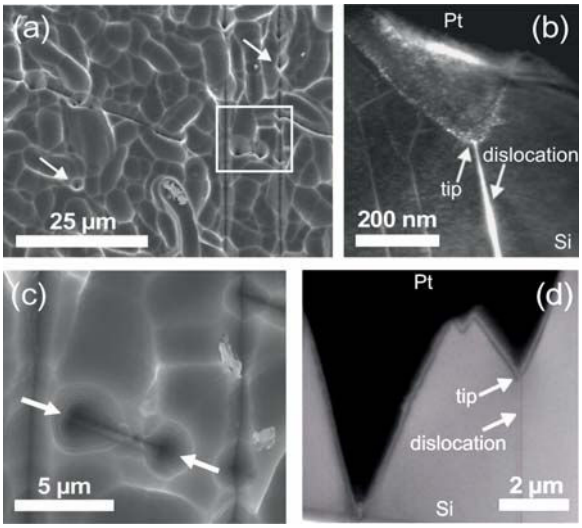

Figure 4 Top-view SEM image of the cell surface showing etch pits (see arrows) (a), weak-beam dark-field TEM image of the tip of an etch pit (b), 20° tilted SEM image of the pair of etch pits marked by the white box in (a) with larger magnification (c), TEM image of the same pair of etch pits (see arrows in (c)) (d). TEM samples were prepared by FIB using Pt as protective layer.

is the case for specific sites, many of them being arranged in lines which intersect under a certain angle. These lines consist of single dots which can be identified by the secondary electron (SE) image as being small holes (cf. the arrows in Fig. 3c, d). In Fig. 3b, the surface of the grain above the grain boundary has no holes, but the surface of the lower grain is defect-rich. Since the surface of the cell was acid-etched for texturization, these holes are most likely etch pits related to dislocations. This supposition is confirmed by scanning electron microscopy (SEM) and transmission electron microscopy (TEM) investigations of the sample section shown in Fig. 3, the results being displayed in Fig. 4.

The SEM image in Fig. 4a shows the cell surface containing cone-shaped holes. Almost all of the holes belonging to a certain grain are uniformly tilted. Figure 4b shows a TEM image of the tip of one of these holes. The sample was prepared using focused ion beam (FIB). The white lines seen in Fig. 4b are dislocations. The tip is connected to one of them and pointing directly along it. This means that the hole was formed along the dislocation, i.e., that it is an etch pit. A magnified SEM image of a pair of such etch pits, inclined according to their tilt of 20°, is shown in Fig. 4c. The same pair is shown in Fig. 4d in a side view (FIB cut between arrows in Fig. 4c). It can be seen that the etch pits are several microns wide and also several microns deep. The planar defect between the arrows in Fig. 4c is a stacking fault bordered by partial dislocations and containing dislocations. Since in the solar cell production process the emitter is being formed by phosphorus in-diffusion after the surface texturization, the p–n junction follows the shape of the etch pits. The radius of curvature at the etch-pit tip is approximately 20 nm, which is one order of magnitude smaller than the emitter thickness of about 250 nm. Therefore the radius of curvature of the p–n junction is determined by the emitter thickness. For such a small radius of curvature of the p–n junction, the electric field becomes significantly enhanced due to the electrostatic tip effect, which leads to a reduction in breakdown voltage. This has been shown theoretically by Sze and Gibbons [15], whose results were confirmed experimentally by Speeney and Carey [16]; it was found that for an abrupt spherical p–n junction, a breakdown voltage of –13 V corresponds to a junction radius of 0.3 µm. This is in excellent agreement with the present data.

We conclude that the electrostatic tip effect quantitatively explains the field enhancement at the bottom of etch pits, thereby enabling avalanche breakdown. Thus, etch pits are identified as a main cause of the hot-spot problem; they have to be avoided by carefully adjusting the etching parameters. This problem will become even more serious whenever material with a doping concentration above 10^{16} cm^{-3} (as, e.g., upgraded metallurgical silicon) is used.

Acknowledgements This work was financially supported by the German Federal Ministry for the Environment (BMU) and all the industry partners within the research cluster SolarFocus (projects 0327650 C and D; www.solarfocus.org). The content of this publication is the responsibility of the authors.

References

[1] M. C. Alonso-García et al., Sol. Energy Mater. Sol. Cells **90**, 329 (2006).
[2] W. Mönch, Phys. Status Solidi **36**, 9 (1969).
S. Mahadevan et al., Phys. Status Solidi A **8**, 335 (1971).
[3] For a p-type doping level of 10^{16} cm^{-3}, the breakdown voltage of an ideal n^+–p junction should exceed –50 V.
S. M. Sze et al., Appl. Phys. Lett. **8**, 111 (1966).
R. M. Warner, Jr., Solid-State Electron. **15**, 1303 (1972).
[4] Y. Kaji et al., Proc. 31st IEEE PVSC, Orlando, USA (2005), p. 1346.
W. Kwapil et al., Proc. 23rd EU-PVSEC, Valencia, Spain (2008), p. 1797.
[5] O. Breitenstein et al., Prog. Photovolt., Res. Appl. **12**, 529 (2004).
[6] O. Breitenstein et al., Prog. Photovolt., Res. Appl. **16**, 679 (2008).
[7] O. Breitenstein and M. Langenkamp, Lock-in Thermography (Springer, Berlin/Heidelberg/New York, 2003).
[8] J.-M. Wagner et al., Proc. 23rd EU-PVSEC,Valencia, Spain (2008), p. 1164.
[9] A. G. Chynoweth et al., Phys. Rev. **102**, 369 (1956).
[10] D. J. Rose, Phys. Rev. **105**, 413 (1957).
[11] A. Goetzberger et al., J. Appl. Phys. **34**, 1591 (1963).
[12] N. Usami et al., Appl. Phys. Express **1**, 075001 (2008).
O. Breitenstein et al., Scanning **30**, 331 (2008).
[13] O. Breitenstein et al., Proc. BIAMS 08, Superlattices Microstruct., accepted (DOI: 10.1016/j.spmi.2008.10.025).
[14] J. W. Bishop, Solar Cells **26**, 335 (1989).
[15] S. M. Sze et al., Solid-State Electron. **9**, 831 (1966).
[16] D. V. Speeney et al., Solid-State Electron. **10**, 177 (1967).

